Supporting Information to

Thermally Persistent Fluorosulfonyl Nitrene and Unexpected Formation of the Fluorosulfonyl Radical

Xiaoqing Zeng,*‡ Helmut Beckers,* Helge Willner

Bergische Universität Wuppertal, FB C – Mathematik und Naturwissenschaften – Fachgruppe Chemie, Wuppertal, Germany.
‡Permanent address: College of Chemistry, Chemical Engineering and Materials Science, Soochow University, 215123 Suzhou (China).

Corresponding Author: zeng@uni-wuppertal.de; beckers@uni-wuppertal.de

Experimental and Computational Methods

Sample Preparation and Photolysis. Fluorosulfonyl azide, FSO_2N_3, was prepared by the reaction of $F_2S_2O_5$ with NaN_3 according to the reported procedure.[1] For the preparation of ^{15}N-labeled FSO_2N_3, 1-^{15}N sodium azide (98 atom % ^{15}N, EURISO-TOP GmbH) was used. For the preparation of ^{18}O-labeled FSO_2N_3, ^{18}O-labeled $F_2S_2O_5$ (60 atom % ^{18}O) was used. The quality of the samples was checked by gas-phase IR spectroscopy. Gas samples (standard grade, Messer-Griesheim, Krefeld, Germany) of CO and O_2 were purified by first liquifying the gases in glass containers and then taking the most volatile part for experiments. Sample of NO was taken directly from a storage vessel and its purity was checked by gas phase IR spectroscopy before use.

Photolysis experiments were performed using a high-pressure mercury lamp (TQ 150, Heraeus) by conducting the light through water-cooled quartz lenses combined with various cutoff or interference filters (Schott), and a Nd^{3+}:YAG laser (266 nm, CryLas, FQSS266-Q2, 10 mW) was also used for photolysis.

Matrix Spectroscopy and Flash Vacuum Pyrolysis. Matrix IR spectra were recorded on a FT-IR spectrometer (IFS 66v/S Bruker) in the reflectance mode using a transfer optic. A KBr beam splitter and an MCT detector were used in the region of 4000 to 500 cm^{-1}. A Ge-coated 6 μm Mylar beam splitter combined with a He(l)-cooled Si bolometer and a CsI window at the cryostat were used in the region of 700–200 cm^{-1}. For each spectrum, 200 scans at a resolution of 0.25 cm^{-1} were co-added.

The gaseous sample was mixed with noble gas in a 1 L stainless-steel storage container. Before the pyrolysis experiment, IR spectrum of the matrix was recorded to make sure that no reaction occurs in the container. Then a small amount of the mixture was passed through a quartz furnace (i.d. 1.0 mm, length 30 mm), which was heated (voltage 4.9 V, current 2.3 A) over a length of ca. 10 mm by a platinum wire (o.d. 0.25 mm, resistance 0.8 Ω), prior to deposition on the cold matrix support (16 K for Ar-matrix, 6 K for Ne-matrix, Rh plated Cu block) in high vacuum. During the pyrolysis experiment, the quartz furnace was overheated and the platinum wire fused, then an aluminium oxide furnace (i.d. 1.0 mm, length 25 mm) was used for the pyrolysis purpose, which can be also heated (voltage 5.6 V, current 2.0 A) to about 1000 K over a length of ca. 10 mm with a tantalum wire (o.d. 0.25 mm, resistance 1.0 Ω). Details of the matrix apparatus have been described elsewhere.[2]

Matrix UV/Vis spectra were measured with the Perkin-Elmer Lambda 900 UV spectrometer in the range of 200 to 700 nm with a data point distance of 0.5 nm and an integration time of 2 seconds. The radiation of the spectrometer was directed into a 150 cm optical quartz fiber, through a quartz lens inside the vacuum shroud and twice passed through the matrix deposit on the cold Rh-plated Cu mirror. A second quartz lens and fiber collected the reflected radiation and returned it to the spectrometer.

Gas-phase IR and Raman Spectroscopy. For the gas-phase IR study, the low-pressure vacuum pyrolysis was performed at a glass vacuum line equipped with a capacitance pressure gauge (221 AHS-1000, MKS Baratron, Burlington, MA), three U-traps and valves with PTFE stems. The vacuum line was connected to an IR gas cell

(optical path length 20 cm, Si windows, 0.6 mm thick), which was fitted into the sample compartment of the FT-IR instrument (Bruker, Vector 22) for measuring gas-phase IR spectra at a resolution of 2 cm^{-1}. The pyrolysis was performed by passing the vapor of liquid FSO_2N_3 (ca. 100 mg, –45 °C) through a quartz tube (14 mm o.d., 6 mm i.d., heated zone 40 mm long), which was filled with quartz wool and heated up to 310 °C. The decomposition of the azide was followed by the pressure of some non-condensable gases passing through three cold U-traps at –65, –110 and –196 °C. After 1 hour of pyrolysis, some white solids were observed in each trap, and the compositions were analyzed by gas-phase IR spectroscopy.

For the low-temperature Raman study, the pyrolysis was performed by passing the vapor of solid FSO_2N_3 (–55 °C) through a heated (500 °C) quartz tube (6 mm o.d., 4 mm i.d., heated zone 20 mm long, distance to the cold-finger 5 cm). The decomposition products were quickly condensed onto the stainless steel cold-finger (–196 °C). The Raman spectra of the solid were recorded on a Bruker-Equinox 55 FRA 106/S FT-Raman spectrometer using a 1064 nm Nd:YAG laser (200 mW), and 200 scans were averaged for each spectrum at a resolution of 2 cm^{-1}.

Computational Details. Geometry optimizations and harmonic frequency calculations were performed using DFT B3LYP[3] method with the 6-311+G(3df) basis set. Complete basis method (CBS-QB3) was also used.[4] Time-dependent (TD) DFT (B3LYP/6-311+G(3df)) calculations[5] were performed for the prediction of UV-vis transitions. All the calculations were performed using the Gaussian 03 software package.[6]

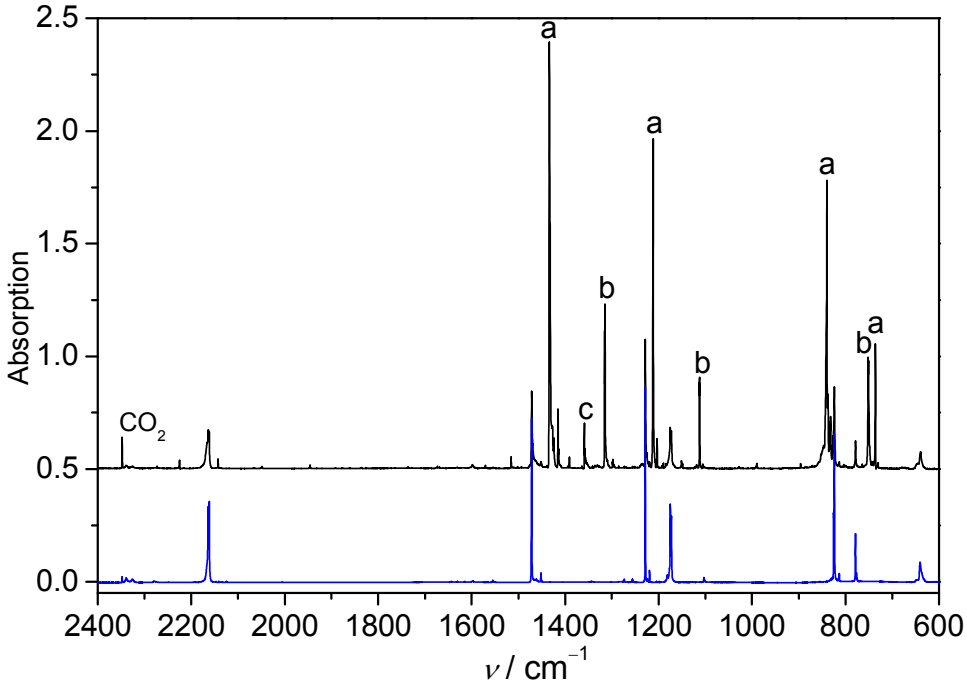

Figure S1. Ar matrix IR spectra (2400–600 cm^{-1}) of FSO_2N_3 (blue line) and its pyrolysis products (black line). Bands of FSO_2N ($^3A''$), FSO_2 ($^2A'$), and SO_2 are marked by a, b, and c, respectively.

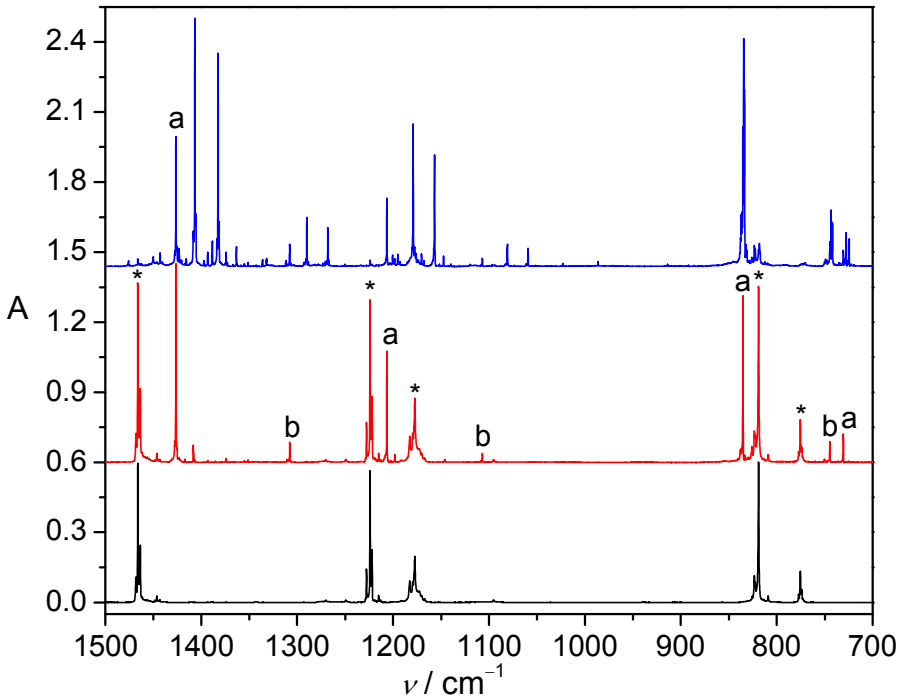

Figure S2. Mid-IR spectra (1500–700 cm^{-1}) of Ar-matrix isolated FSO_2N_3 (bottom, black line), its pyrolysis products (middle, red line), and pyrolysis products of a 1:2.7:1.9 mixture of $FS(^{16}O)_2N_3$, $FS(^{16}O)(^{18}O)N_3$, and $FS(^{18}O)_2N_3$ (top, blue line). Bands of FSO_2N ($^3A''$) and FSO_2 ($^2A'$) are marked by a and b, respectively. Bands of FSO_2N_3 are marked by asterisks.

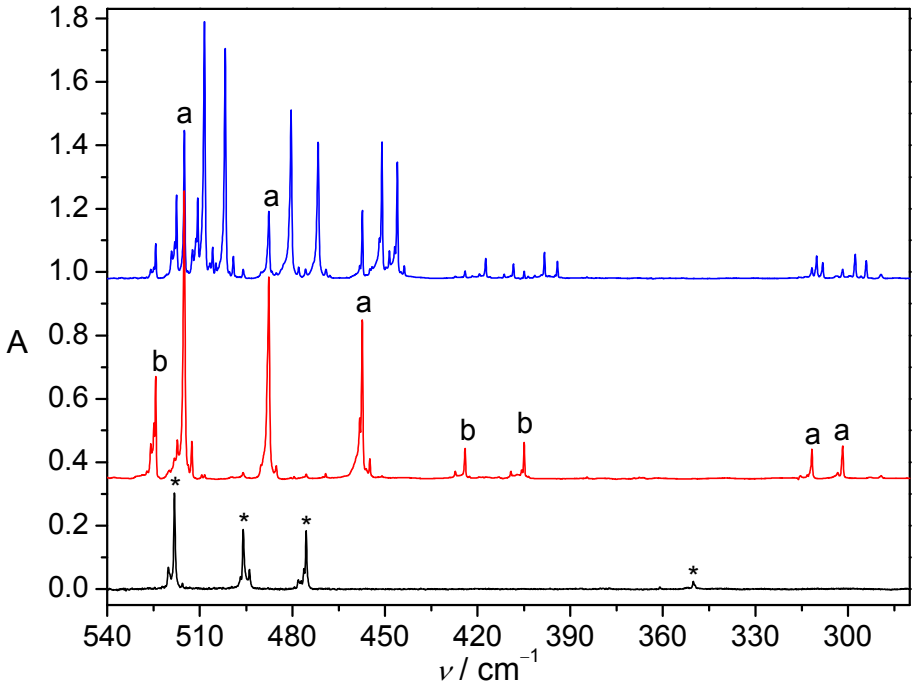

Figure S3. Far-IR spectra (540–280 cm^{-1}) of Ar-matrix isolated FSO_2N_3 (bottom, black line), its pyrolysis products (middle, red line), and pyrolysis products of a 1:2.7:1.9 mixture of $FS(^{16}O)_2N_3$, $FS(^{16}O)(^{18}O)N_3$, and $FS(^{18}O)_2N_3$ (top, blue line). Bands of FSO_2N ($^3A''$) and FSO_2 ($^2A'$) are marked by a and b, respectively. Bands of FSO_2N_3 are marked by asterisks.

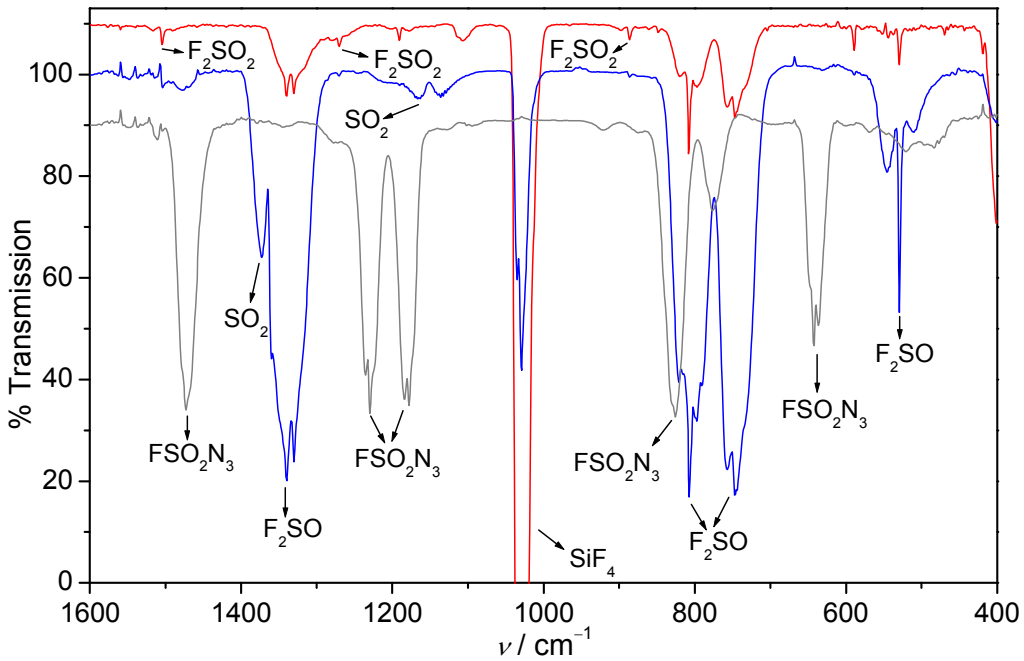

Figure S4. Gas-phase IR spectra of the FSO_2N_3 precursor (grey line), its most volatile pyrolysis products, which retained in a –196 °C trap (red line), and the less volatile pyrolysis products also trapped in the same –196 °C trap (blue line). The grey and red lines are shifted for better illustration.

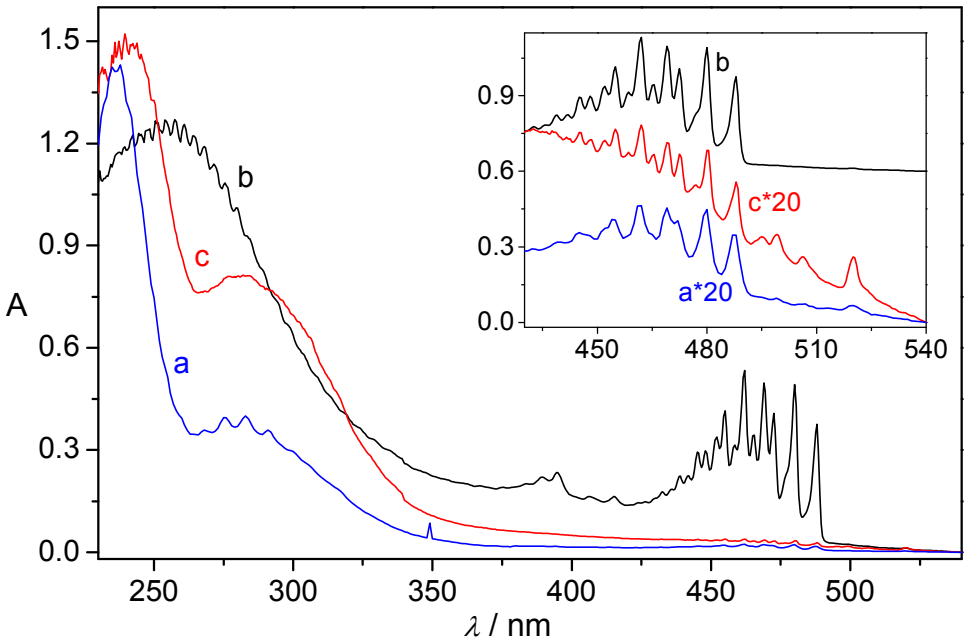

Figure S5. Ne matrix UV/Vis spectra obtained from a) ArF laser (λ = 193 nm) photolysis products of FSO_2N_3, b) pyrolysis products of FSO_2N_3, and c) after UV (λ = 266 nm) photolysis of b. The vibrational structure of the band in the visible region (430–500 nm) is associated with the $A^3A'' \leftarrow X^3A''$ transition of FSO_2N,[7] while, the superimposed vibrational structure of the UV band, λ_{max} = 260 nm in spectrum b is tentatively assigned to FSO_2, as this structure was not observed in the UV/Vis spectrum of the photolysis products of the azide (a). The nitrene FSO_2N also contributes partially to this broad UV band, as indicated by its strong depletion upon 266 nm irradiation. In spectrum c, the bands at λ_{max} = 285 and 240 nm are mainly contributed by FS(O)NO.[7]

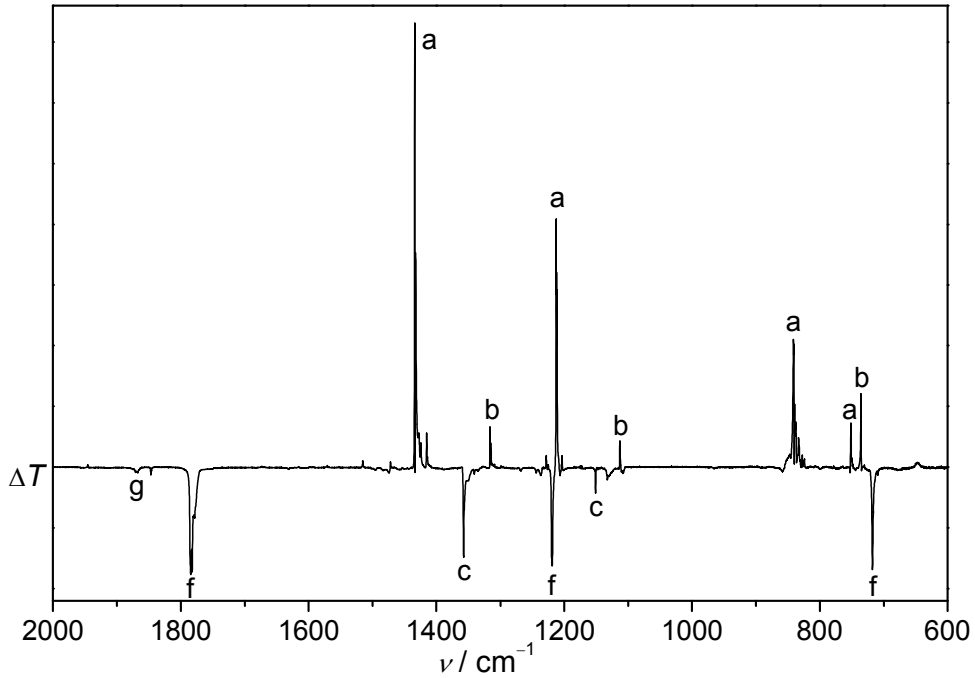

Figure S6. Ne-matrix IR spectra showing the depletion of bands due to FSO_2N ($^3A''$, a) and FSO_2 ($^2A'$, b) upon UV irradiation (λ = 266 nm), and the simultaneous formation of SO_2 (c), FS(O)NO (f), and FNO (g).

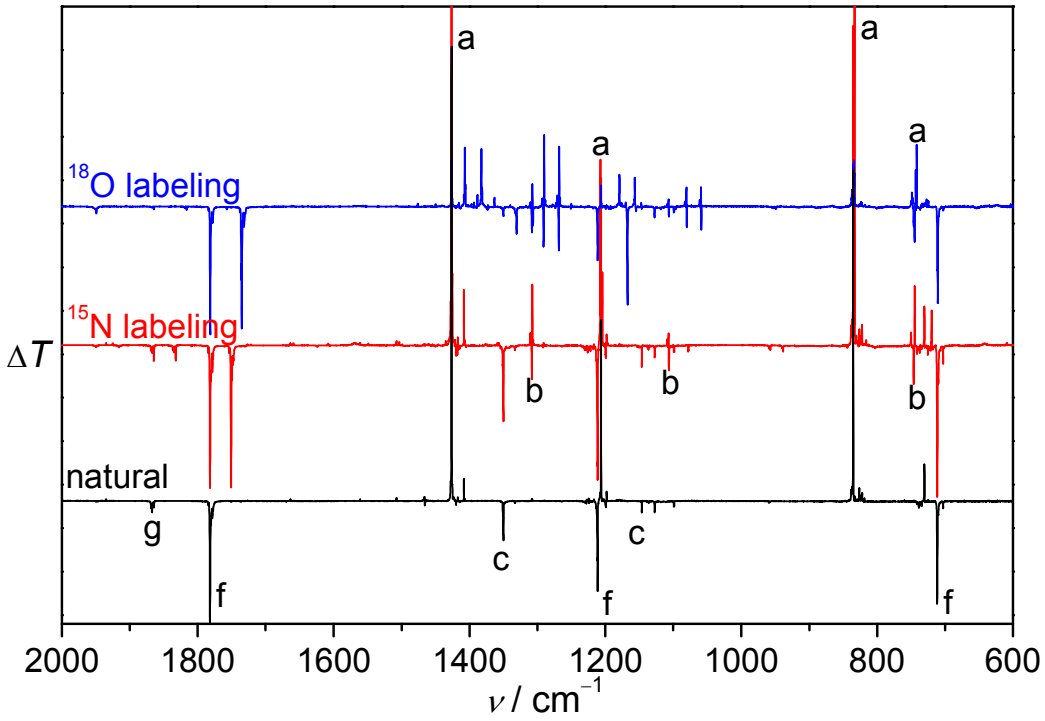

Figure S7. IR spectral changes in the region of 2000–600 cm^{-1} obtained after irradiation (λ > 320 nm) of the pyrolysis products of FSO_2N_3 (bottom trace), a 1:1 mixture of $FSO_2{}^{15}NNN$ and $FSO_2NN^{15}N$ (middle trace), and 1:2.7:1.9 mixture of $FS(^{16}O)_2N_3$, $FS(^{16}O)(^{18}O)N_3$, and $FS(^{18}O)_2N_3$ (top trace). Bands of FSO_2N (^{3}A"), FSO_2 (^{2}A'), SO_2, FS(O)NO, and FNO are marked by a, b, c, f, and g, respectively.

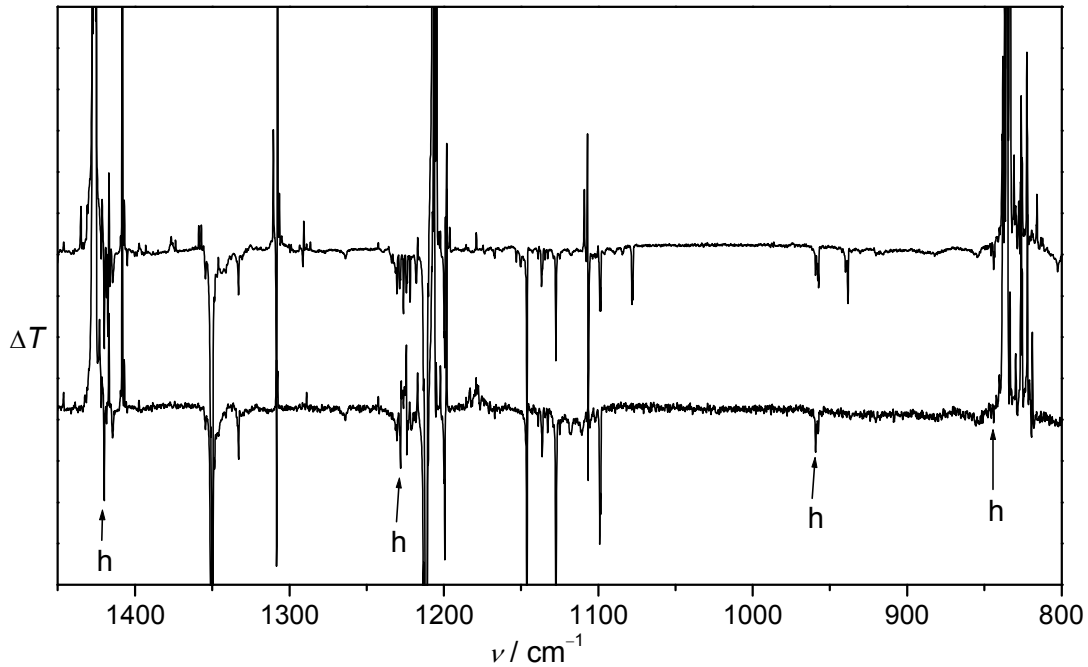

Figure S8. IR spectral changes in the region of 1500–600 cm^{-1} obtained after irradiation (λ > 320 nm) of the pyrolysis products of FSO_2N_3 (lower trace), a 1:1 mixture of $FSO_2{}^{15}NNN$ and $FSO_2NN^{15}N$ (upper trace). The bands of $FNSO_2$ are marked by arrowhead and labeled by h.

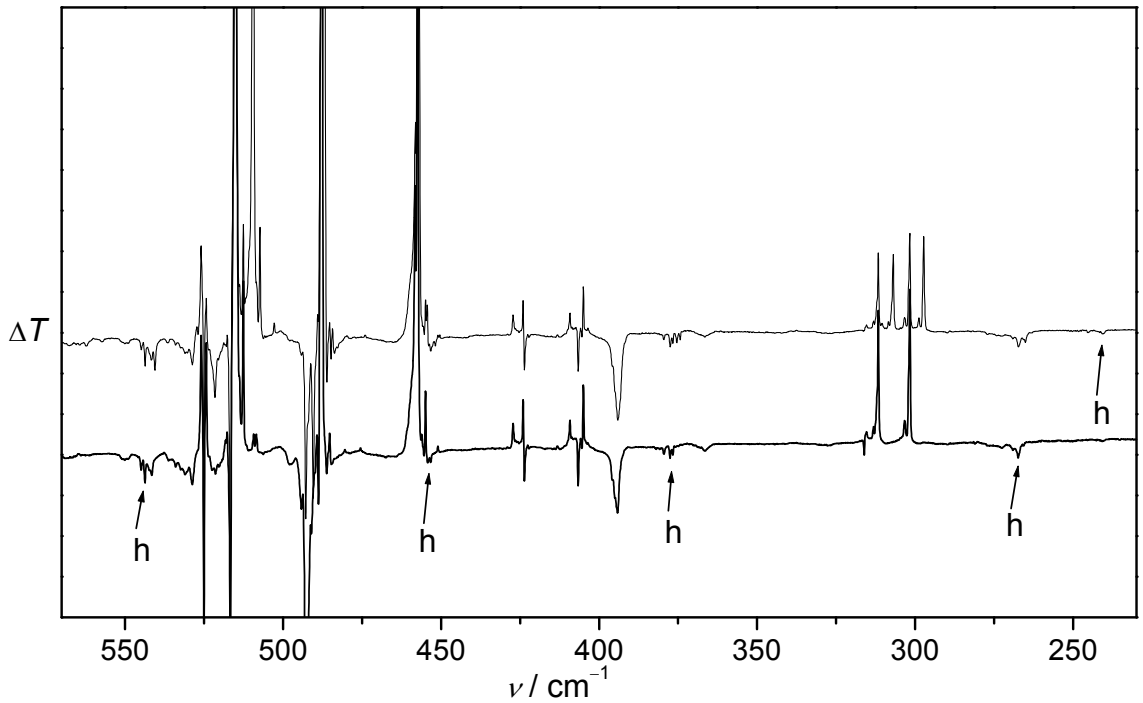

Figure S9. IR spectral changes in the region of 570–230 cm^{-1} obtained after irradiation (λ > 320 nm) of the pyrolysis products of FSO_2N_3 (lower trace), a 1:1 mixture of $FSO_2{}^{15}NNN$ and $FSO_2NN^{15}N$ (upper trace). The bands of $FNSO_2$ are marked by arrowhead and labeled by h.

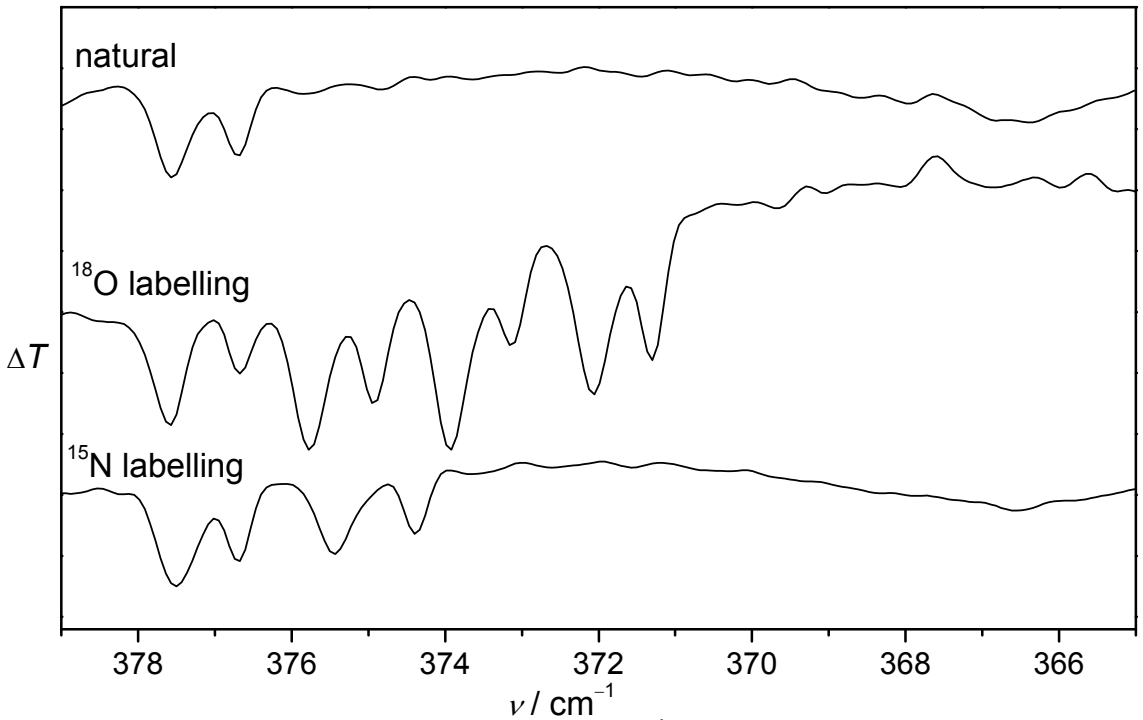

Figure S10. IR spectral changes in the region of 379–365 cm^{-1} obtained after irradiation (λ > 320 nm) of the pyrolysis products of FSO_2N_3 (top trace), a 1:2.7:1.9 mixture of $FS(^{16}O)_2N_3$, $FS(^{16}O)(^{18}O)N_3$, and $FS(^{18}O)_2N_3$ (middle trace), and a 1:1 mixture of $FSO_2{}^{15}NNN$ and $FSO_2NN^{15}N$ (lower trace), these IR bands are assigned to $FNSO_2$.

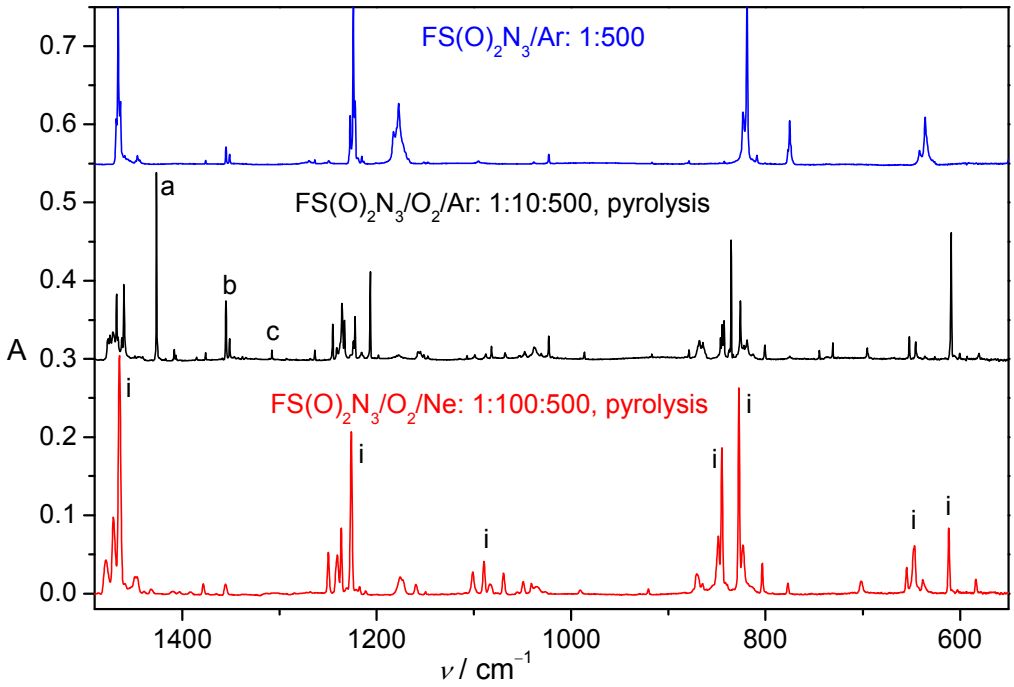

Figure S11. Matrix IR spectra of FSO_2N_3/Ar (1:500, upper trace), pyrolysis products of FSO_2N_3/O_2/Ar (1:10:500, middle trace), and pyrolysis products of FSO_2N_3/O_2/Ne (1:100:500, lower trace). The bands of FSO_2N (^{3}A"), FSO_2 (^{2}A'), SO_2, and FSO_2NOO are marked by a, b, c, and i, respectively.

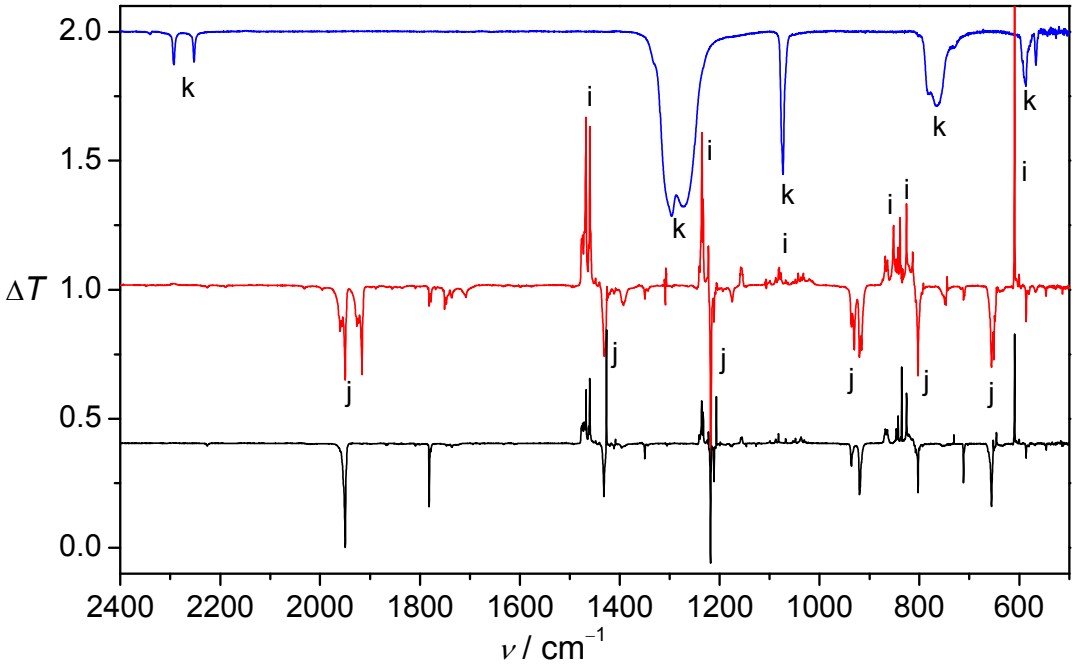

Figure S12. IR spectral changes in the region of 2400–500 cm^{-1} obtained after irradiation (λ > 320 nm) of the pyrolysis products of FSO_2N_3/O_2/Ar mixtures (1:10:500): natural FSO_2N_3 (bottom trace), 1:1 mixture of $FSO_2{}^{15}NNN$ and $FSO_2NN{}^{15}N$ (middle trace). IR spectrum of the solid residue (top trace) after warming up the matrix to room temperature which contains the products after irradiation (λ > 320 nm) of the pyrolysis products of $FSO_2{}^{15}NNN/FSO_2NN{}^{15}N/O_2$/Ar (1:1:20:1000). The bands of FSO_2NOO, $FS(O)_2ONO$, and $NO^+SO_3F^-$ are marked by i, j, and k, respectively.

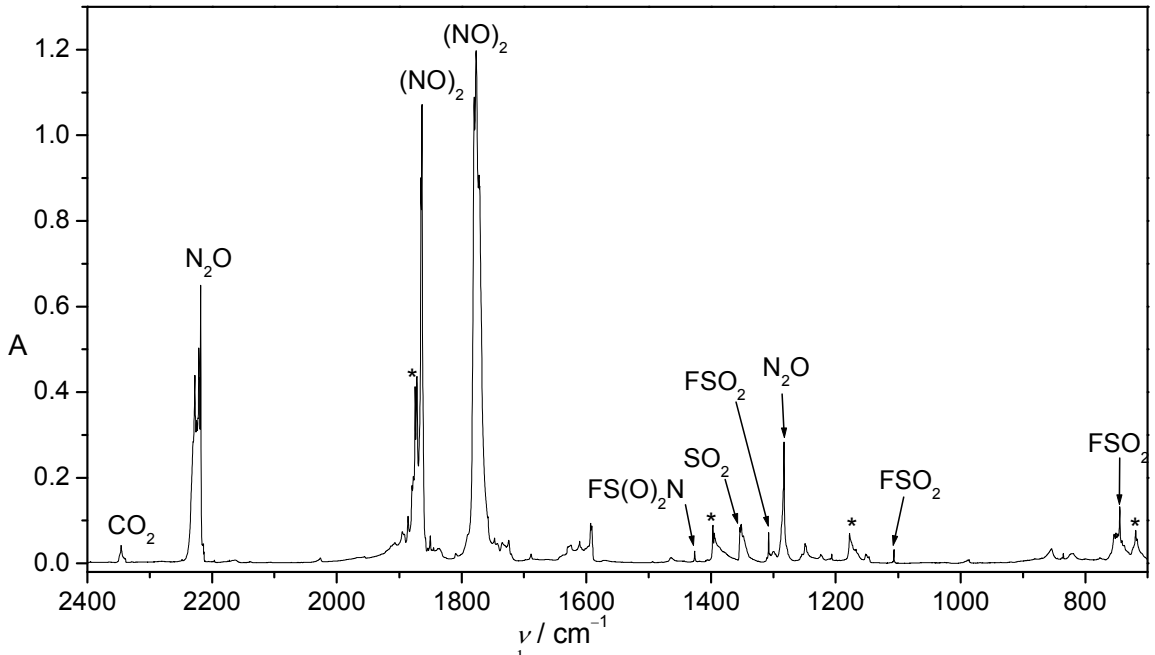

Figure S13. Ar matrix IR spectra (2400–700 cm^{-1}) of the pyrolysis products of FSO_2N_3/NO/Ar (1:15:500). The bands of FSO_2NO are marked by asterisks.

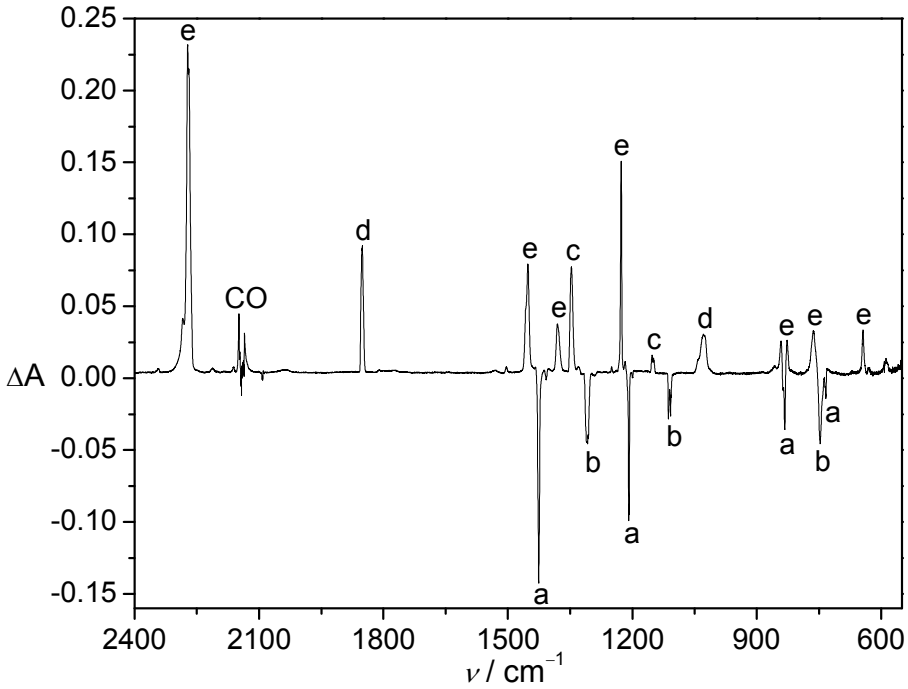

Figure S14. IR spectral changes in the region of 2400–550 cm^{-1} obtained after visible irradiation (λ > 420 nm) of the Ar-matrix isolated pyrolysis products of FSO_2N_3/CO/Ar mixture (1:20:200). Bands of depleted (pointing downward) species FSO_2N ($^3A''$) and FSO_2 ($^2A'$) are marked by a, b, respectively, while bands of newly formed (pointing upward) species SO_2, FCO,[8] and FSO_2NCO[9] are marked by c, d, and e, respectively.

Table S1. Calculated and Experimentally Observed IR Frequencies (cm^{-1}) and Isotopic Shifts (cm^{-1}) of $FNSO_2$.

frequencies			$^{14/15}N$[d]		approx. assignment[e]
calcd[a]	exptl (Ar)[b]	exptl (Ne)[c]	calcd	exptl	
1430 (171)	1420.0 s	1420.1	0.1	2.3	A', ν_1/SO_2 asym. stretch
1244 (94)	1230.4 m	1231.4	4.8	4.2	A', ν_2/SO_2 sym. stretch
994 (95)	959.2 m	959.3	20.0	19.3	A', ν_3/NF stretch
857 (34)	844.2 w	841.4	17.6	17.0	A', ν_4/SN stretch
551 (21)	543.6 w		3.4	3.1	A", ν_5/OSN bending
456 (12)	453.3 w		1.5	1.4	A', ν_6/SO_2 bending
240 (5)	240.9 vw		0.2	< 0.5	A', ν_7/$FNSO_2$ i.p. deformation
384 (18)	377.5 w		2.4	2.1	A", ν_8/NSO_2 o.o.p. deformation
245 (1)	245.5 vvw		3.4	-[f]	A", ν_9/FNSO o.o.p. deformation

[a] DFT B3LYP/6-311+G(3df) calculated frequencies and IR intensities (km mol^{-1}, in parentheses). [b] Observed IR band positions in Ar-matrix (16 K) of the most-intense matrix sites and relative intensities (in parentheses), s strong, m medium, w weak, vw very weak, vvw very very weak. [c] Observed mid-IR band positions in Ne-matrix (6 K). [d] The calculated and observed isotopic shifts are given relative to $F^{14}NSO_2$. [e] Approximate descriptions of mode according to the calculated displacement vectors, i.p. in-plane, o.o.p. out-of-plane. [f] No isotopic shift was observed due to the rather low intensity.

Table S2. Calculated and experimentally observed IR frequencies (cm^{-1}) and isotopic shifts (cm^{-1}) of singlet FSO_2NOO. The calculated IR frequencies (cm^{-1}) of *cyc*-$FS(O)_2ONO$ and FSO_2NO_2 are also given for comparison.

calculated harmonic frequencies [a]					experimental		$^{14/15}N$ isotopic shifts[d]	
triplet (^3A)	singlet (^1A)				FSO_2NOO (^1A)		FSO_2NOO (^1A)	
anti-FSO_2NOO	*anti*-FSO_2NOO	*syn*-FSO_2NOO	*cyc*-FSO_2ONO	FSO_2NO_2	Ar-matrix[b]	Ne-matrix[c]	calcd	exptl
1471 (214)	1477 (210)	1471 (209)	1478 (223)	1722 (359)	1459.8	1464.6	0.1	< 0.5
1231 (164)	1244 (45)	1239 (98)	1242 (131)	1473 (164)	1235.8	1236.4	0.8	0.6
1013 (5)	1241 (79)	1199 (107)	1214 (36)	1366 (143)	1222.3	1225.9	7.7	
869 (16)	1168 (276)	1152 (132)	849 (12)	1223 (190)	1157.5	1159.6	13.8	
783 (227)	869 (50)	853 (19)	815 (148)	844 (56)	868.5	870.0	18.7	16.7
721 (62)	799 (222)	783 (138)	793 (3)	756 (211)	826.0	827.4	0.6	< 0.5
579 (101)	600 (185)	624 (118)	648 (43)	655 (18)	609.3	611.5	0.1	< 0.5
496 (15)	509 (8)	541 (9)	561 (63)	584 (136)			1.1	
472 (12)	498 (13)	461 (8)	507 (10)	480 (9)			1.8	
356 (0.2)	404 (6)	446 (12)	459 (17)	451 (16)			3.6	
338 (0.6)	359 (1)	425 (7)	394 (3)	357 (2)			2.6	
285 (0.8)	344 (1)	301 (2)	325 (1)	253 (10)			1.8	
169 (1)	219 (6)	217 (1)	217 (2)	196 (2)			0.3	
120 (0.8)	198 (2)	192 (0.2)	213 (1)	187 (2)			0.4	
81 (0.1)	43 (1)	115 (0.4)	86 (0.2)	16 (0.1)			0.6	

[a] DFT B3LYP/6-311+G(3df) calculated IR frequencies and intensities (km mol^{-1}, in parentheses). [b] Observed IR band positions of $FSO_2{}^{14}NOO$ in Ar matrix (16 K) of the main matrix sites. [c] Observed mid-IR band positions of $FSO_2{}^{14}NOO$ in Ne-matrix (6 K). [d] The calculated and observed isotopic shifts are given relative to $FSO_2{}^{14}NOO$.

Table S3. Calculated and experimentally observed IR frequencies (cm^{-1}) and isotopic shifts (cm^{-1}) of $FS(O)_2ONO$.

frequencies						$^{14/15}N$ isotopic shifts[f]	
calcd[a]	calcd[a]	exptl[b]	exptl[c]	exptl[d]	exptl[d]	calcd	exptl
anti	*syn*	Ar-matrix	Ne-matrix	solid, this work	solid, ref[10]		
2050 (560)	2115 (523)	1949.5	1959.0	2293 m	2300 ms	36.3	33.6
1443 (239)	1416 (219)	1432.0	1434.7	1296–1291 vs, br	1300–1260 vs, br	0.0	< 0.5
1226 (226)	1206 (175)	1218.2	1221.9	1074 vs	1075 vs	0.2	< 0.5
915 (214)	909 (307)	919.8	919.4			3.0	3.9
777 (182)	773 (192)	802.7	805.7	764 vs, br	745 vs, br	0.1	< 0.5
657 (427)	636 (8)	655.8	658.1			5.7	4.9
577 (15)	587 (73)	587.0	587.1	587 m, br	596 m, sh; 591 s	0.2	< 0.5
534 (12)	537 (11)	546.5	548.2	567 m	568 s	0.0	< 0.5
507 (18)	513 (79)				420mw, sh	4.0	
400 (14)	418 (20)				405 w	0.3	
374 (< 1)	374 (1)					0.1	
273 (134)	261 (66)					3.0	
148 (< 1)	169 (2)					0.9	
88 (< 1)	130 (< 1)					1.4	
53 (1)	42 (1)					0.4	

[a] DFT B3LYP/6-311+G(3df) calculated IR frequencies and intensities (km mol^{-1}, in parentheses). [b] Observed IR band positions in Ar-matrix (16 K) of the most-intense matrix sites. [c] Observed mid-IR band positions in Ne-matrix (6 K). [d] Observed IR band positions of the solid residue after warming up the matrix to room temperature. Relative intensities, vs very strong, ms medium strong, s strong, w weak, br broad, sh shoulder. [f] The calculated and observed isotopic shifts are given relative to $FS(O)_2O^{14}NO$.

Table S4. Calculated IR frequencies (cm^{-1}) of FSO_2NO. The calculated IR frequencies (cm^{-1}) of $FS(O)_2OO$ and FSO_2NNO are also given for comparison.

FSO_2NO		$FS(O)_2OO$	*anti*-FSO_2NNO	*syn*-FSO_2NNO
calcd[a]	exptl (Ar)[b]			
1879 (569)	1871.8 s	1500 (224)	1697 (374)	1717 (482)
1400 (234)	1394.7 m	1249 (149)	1475 (239)	1452 (227)
1186 (147)	1178.0 m	1118 (14)	1331 (83)	1286 (3)
720 (227)	718.3 m	813 (193)	1236 (193)	1222 (106)
640 (27)		650 (64)	848 (63)	824 (236)
564 (60)	569.5 w	579 (75)	790 (193)	770 (26)
432 (6)		491 (19)	608 (196)	607 (133)
392 (11)		452 (13)	515 (11)	562 (12)
194 (66)		365 (0.2)	506 (10)	482 (11)
165 (1)		328 (0.3)	415 (3)	437 (7)
124 (1)		233 (1)	376 (3)	433 (3)
67 (1)		88 (0.3)	356 (1)	299 (1)
			268 (5)	271 (1)
			185 (1)	152 (0.3)
			36 (0.4)	12 (0.1)

[a] DFT B3LYP/6-311+G(3df) calculated frequencies and IR intensities (km mol^{-1}, in parentheses). [b] Observed IR band positions in Ar-matrix (16 K) of the most-intense matrix sites and relative intensities (in parentheses), s strong, m medium, w weak.

Table S5. Vertical excitation energies (λ), oscillator strength (f), and major configurations (>20%) for the lowest-energy electronic transitions of $FNSO_2$ and FSO_2 ($^2A'$) calculated at the TD-DFT (B3LYP/6-311+G(3df)) level of theory.

$FNSO_2$			FSO_2 ($^2A'$)		
λ (nm)	f	major configurations	λ (nm)	f	major configurations
264	0.0015	100%: 24 → 25	484	0.0001	90%: 20→ 21
227	0.0105	51%: 23 → 25 49%: 24 → 26	412	0.0104	85%: 19→ 21
211	0.0006	58%: 23 → 26 42%: 24 → 27	303	0.0056	100%: 18→21
204	0.0019	43%: 23 → 26 57%: 24 → 27	241	0.0128	95%:17→21

****

Calculated Atomic Coordinates (in Angstroms) and Energies (in Hatrees) for All Optimized Structures at the B3LYP/6-311+G(3df) Level of Theory

$FNSO_2$

S	0.00000000	0.44779700	0.00000000
O	1.42489400	0.49303500	0.00000000
O	-0.84241300	1.59740100	0.00000000
N	-0.80021400	-0.89471400	0.00000000
F	0.10462800	-1.95836100	0.00000000

Zero-point correction= 0.014586
Thermal correction to Energy= 0.019306
Thermal correction to Enthalpy= 0.020250
Thermal correction to Gibbs Free Energy= -0.013704
Sum of electronic and zero-point Energies= -703.208579
Sum of electronic and thermal Energies= -703.203859
Sum of electronic and thermal Enthalpies= -703.202915
Sum of electronic and thermal Free Energies= -703.236869

FSO_2 (^{2}A')

S	0.02234900	-0.13824100	0.25321500
F	-0.22614000	1.40597700	-0.11247400
O	-1.14439600	-0.85303400	-0.18990900
O	1.35410600	-0.45220800	-0.18998800

Zero-point correction= 0.010180
Thermal correction to Energy= 0.013976
Thermal correction to Enthalpy= 0.014920
Thermal correction to Gibbs Free Energy= -0.017211
Sum of electronic and zero-point Energies= -648.537562
Sum of electronic and thermal Energies= -648.533766
Sum of electronic and thermal Enthalpies= -648.532822
Sum of electronic and thermal Free Energies= -648.564952

FSO_2NO

F	0.00000000	0.00000000	0.00000000
O	0.00000000	0.00000000	2.43383617
S	0.90753954	0.00000000	1.33024535
O	1.91107366	1.00129768	1.14055470
N	1.70820165	-1.91492400	0.96650930
O	2.82364169	-1.84649344	0.75891955

Zero-point correction= 0.017697
Thermal correction to Energy= 0.024249
Thermal correction to Enthalpy= 0.025194
Thermal correction to Gibbs Free Energy= -0.013773
Sum of electronic and zero-point Energies= -778.496701
Sum of electronic and thermal Energies= -778.490148
Sum of electronic and thermal Enthalpies= -778.489204
Sum of electronic and thermal Free Energies= -778.528171

***syn*-FSO_2NOO (^{1}A)**

N	0.61003900	1.13378700	0.02056300

F	-0.43266400	-0.86326100	-1.17417800
O	-0.58159700	-0.83964300	1.24591300
S	-0.71223800	-0.00773700	0.10903600
O	-1.84582600	0.78970900	-0.16184400
O	1.78180800	0.65134100	0.01223200
O	2.02305400	-0.60682700	-0.01141600

Zero-point correction= 0.022842
Thermal correction to Energy= 0.029257
Thermal correction to Enthalpy= 0.030202
Thermal correction to Gibbs Free Energy= -0.008079
Sum of electronic and zero-point Energies= -853.603326
Sum of electronic and thermal Energies= -853.596911
Sum of electronic and thermal Enthalpies= -853.595967
Sum of electronic and thermal Free Energies= -853.634248

anti-FSO_2NOO (^1A)

N	-0.77604300	-0.68412600	-0.04566200
F	1.26536700	-0.47097300	1.26964800
O	1.49784400	-0.62695100	-1.11462900
S	0.78575000	0.07722000	-0.11749500
O	0.71307100	1.48667400	-0.02137900
O	-1.65533400	0.23984700	-0.01557500
O	-2.87158100	-0.12555700	-0.00182700

Zero-point correction= 0.022735
Thermal correction to Energy= 0.029326
Thermal correction to Enthalpy= 0.030270
Thermal correction to Gibbs Free Energy= -0.009123
Sum of electronic and zero-point Energies= -853.604524
Sum of electronic and thermal Energies= -853.597934
Sum of electronic and thermal Enthalpies= -853.596989
Sum of electronic and thermal Free Energies= -853.636382

FSO_2NOO (^3A)

N	-0.73088200	-0.74175600	-0.08262300
F	0.91706800	0.42363300	1.38139600
O	1.69290200	-1.09895700	-0.31620900
S	0.80689000	-0.01364000	-0.12956400
O	0.82184000	1.17774000	-0.89548700
O	-1.62571600	0.27829600	-0.02315300
O	-2.89498600	-0.15735000	0.01220100

Zero-point correction= 0.020485
Thermal correction to Energy= 0.027508
Thermal correction to Enthalpy= 0.028452
Thermal correction to Gibbs Free Energy= -0.012569
Sum of electronic and zero-point Energies= -853.567942
Sum of electronic and thermal Energies= -853.560919
Sum of electronic and thermal Enthalpies= -853.559975
Sum of electronic and thermal Free Energies= -853.600997

syn-$FS(O)_2ONO$

F	-0.49160600	1.37788300	-0.38905900

O	-2.04613100	-0.51601400	-0.10367500
S	-0.79202000	-0.03302100	0.39704800
O	2.15965600	0.41641700	0.31198200
O	0.33679000	-0.89475600	-0.38749200
N	1.92774900	-0.55968300	-0.20253600

Zero-point correction= 0.022995
Thermal correction to Energy= 0.029946
Thermal correction to Enthalpy= 0.030890
Thermal correction to Gibbs Free Energy= -0.009338
Sum of electronic and zero-point Energies= -853.743599
Sum of electronic and thermal Energies= -853.736648
Sum of electronic and thermal Enthalpies= -853.735704
Sum of electronic and thermal Free Energies= -853.775932

***anti*-$FS(O)_2ONO$**

F	-1.04122700	1.38976900	-0.25550200
O	-1.86723400	-0.92325700	-0.25661300
S	-0.88022000	-0.10592100	0.38612600
O	2.72024300	-0.10226900	-0.19059500
O	0.51502600	-0.45480300	-0.38279400
N	1.78718400	0.14706400	0.39450300

Zero-point correction= 0.022851
Thermal correction to Energy= 0.029893
Thermal correction to Enthalpy= 0.030837
Thermal correction to Gibbs Free Energy= -0.009749
Sum of electronic and zero-point Energies= -853.745361
Sum of electronic and thermal Energies= -853.738319
Sum of electronic and thermal Enthalpies= -853.737375
Sum of electronic and thermal Free Energies= -853.777961

FSO_2NO_2

N	-1.25343800	0.01102400	-0.04487300
F	0.87654700	-0.44871700	1.35548400
O	1.11353100	-0.99178300	-0.98767900
S	0.68853300	0.04682500	-0.12518500
O	1.10826500	1.39572900	-0.19139000
O	-1.77008300	1.08853700	-0.03549000
O	-1.71813500	-1.09097400	-0.02072700

Zero-point correction= 0.024078
Thermal correction to Energy= 0.030793
Thermal correction to Enthalpy= 0.031737
Thermal correction to Gibbs Free Energy= -0.008715
Sum of electronic and zero-point Energies= -853.715440
Sum of electronic and thermal Energies= -853.708726
Sum of electronic and thermal Enthalpies= -853.707781
Sum of electronic and thermal Free Energies= -853.748233

***cyclic* FSO_2NO_2**

N	-0.92782200	0.00003300	-0.78676800
F	0.39868500	-0.00007000	1.44954100
O	1.27652200	-1.25283800	-0.41698900

S	0.71230800	0.00000700	-0.08346400
O	1.27646600	1.25291600	-0.41683500
O	-1.80718100	0.73021500	0.02920400
O	-1.80709900	-0.73025800	0.02923500

Zero-point correction= 0.022345
Thermal correction to Energy= 0.028763
Thermal correction to Enthalpy= 0.029707
Thermal correction to Gibbs Free Energy= -0.008671
Sum of electronic and zero-point Energies= -853.595661
Sum of electronic and thermal Energies= -853.589243
Sum of electronic and thermal Enthalpies= -853.588299
Sum of electronic and thermal Free Energies= -853.626678

$FS(O)_2OO$

F	0.42450600	0.37888800	1.40176900
O	1.38627200	-1.00072800	-0.32600200
S	0.44716800	0.03023600	-0.11896500
O	0.37068600	1.23969000	-0.83835500
O	-2.07218600	0.04633600	-0.01481400
O	-1.05667800	-0.77202000	-0.15988900

Zero-point correction= 0.017932
Thermal correction to Energy= 0.023676
Thermal correction to Enthalpy= 0.024621
Thermal correction to Gibbs Free Energy= -0.012723
Sum of electronic and zero-point Energies= -798.920998
Sum of electronic and thermal Energies= -798.915254
Sum of electronic and thermal Enthalpies= -798.914310
Sum of electronic and thermal Free Energies= -798.951654

***anti*-FSO_2NNO**

F	1.12275400	-0.21261600	1.37835100
O	1.59109800	-0.78131500	-0.90652600
S	0.76579500	0.05837700	-0.12722900
O	0.67770400	1.46261100	-0.28799600
O	-2.89017400	-0.04309300	0.00186700
N	-1.71522000	0.10849400	-0.02081700
N	-0.76857000	-0.69793800	-0.09750700

Zero-point correction= 0.024263
Thermal correction to Energy= 0.030750
Thermal correction to Enthalpy= 0.031694
Thermal correction to Gibbs Free Energy= -0.008245
Sum of electronic and zero-point Energies= -833.234249
Sum of electronic and thermal Energies= -833.227762
Sum of electronic and thermal Enthalpies= -833.226818
Sum of electronic and thermal Free Energies= -833.266756

***syn*-FSO_2NNO**

F	1.75122600	0.88381700	-0.20335700
O	0.76616500	-0.68527300	1.32811900
S	0.61766700	-0.16613100	0.01819500
O	0.54350300	-0.97009400	-1.14700200

O	-2.37537700	-0.44333200	0.00333100
N	-1.79392700	0.60103800	0.00291000
N	-0.65150700	1.04086700	0.00616400

Zero-point correction= 0.024002
Thermal correction to Energy= 0.030588
Thermal correction to Enthalpy= 0.031532
Thermal correction to Gibbs Free Energy= -0.009476
Sum of electronic and zero-point Energies= -833.228137
Sum of electronic and thermal Energies= -833.221551
Sum of electronic and thermal Enthalpies= -833.220606
Sum of electronic and thermal Free Energies= -833.261615

***anti*-FSO_2NNSO_2F**

S	1.47428300	-1.48274600	0.09328600
O	2.55509300	-0.73212400	-0.42583300
O	1.47428300	-2.14509900	1.34365700
F	1.04058500	-2.51507100	-0.99880800
O	-2.55509300	0.73212400	-0.42583300
O	-1.47428300	2.14509900	1.34365700
F	-1.04058500	2.51507100	-0.99880800
S	-1.47428300	1.48274600	0.09328600
N	0.08591800	0.59991600	0.02201400
N	-0.08591800	-0.59991600	0.02201400

Zero-point correction= 0.033991
Thermal correction to Energy= 0.043884
Thermal correction to Enthalpy= 0.044828
Thermal correction to Gibbs Free Energy= -0.003002
Sum of electronic and zero-point Energies= -1406.600453
Sum of electronic and thermal Energies= -1406.590561
Sum of electronic and thermal Enthalpies= -1406.589617
Sum of electronic and thermal Free Energies= -1406.637447

***syn*-FSO_2NNSO_2F**

S	1.62802400	-0.16783100	-0.02195100
O	1.35846300	-0.93534600	1.14013000
O	1.78515400	-0.68787800	-1.33118500
F	2.89593700	0.69696800	0.28599300
O	-2.10091700	-0.17480400	1.42046800
O	-2.77482400	0.31293100	-0.94260900
F	-0.99500800	-1.23947900	-0.46537600
S	-1.81222700	0.01217400	0.04782600
N	-0.62045200	1.39014200	-0.06422900
N	0.57700700	1.36041300	-0.09205500

Zero-point correction= 0.033044
Thermal correction to Energy= 0.043231
Thermal correction to Enthalpy= 0.044175
Thermal correction to Gibbs Free Energy= -0.004863
Sum of electronic and zero-point Energies= -1406.587310
Sum of electronic and thermal Energies= -1406.577123
Sum of electronic and thermal Enthalpies= -1406.576179
Sum of electronic and thermal Free Energies= -1406.625218
****

References:

[1] Zeng, X. Q.; Gerken, M.; Beckers, H.; Willner, H. *J. Phys. Chem. A*, **2010**, *114*, 7624–7630.

[2] Schnöckel, H. G.; Willner, H. In *Infrared and Raman Spectroscopy, Methods and Applications;* Schrader, B., Ed.; VCH: Weinheim, 1994.

[3] Becke, A. D. *J. Chem. Phys.* **1993**, *98*, 5648–5652.

[4] Montgomery Jr., J. A.; Frisch, M. J.; Ochterski, J. W.; Petersson, G. A. *J. Chem. Phys.* **2000**, *112*, 6532–6542.

[5] (a) Stratmann, R. E.; Scuseria, G. E.; Frisch, M. J. *J. Chem. Phys.* **1998**, *109*, 8218–8224. (b) Foresman, J. B.; Head-Gordon, M.; Pople, J. A.; Frisch, M. J. *J. Phys. Chem.* **1992**, *96*, 135–149.

[6] Frisch, M. J.; Trucks, G. W.; Schlegel, H. B.; Scuseria, G. E.; Robb, M. A.; Cheeseman, J. R.; Montgomery, J. A. Jr.; Vreven, T.; Kudin, K. N.; Burant, J. C.; Millam, J. M.; Iyengar, S. S.; Tomasi, J.; Barone, V.; Mennucci, B.; Cossi, M.; Scalmani, G.; Rega, N.; Petersson, G. A.; Nakatsuji, H.; Hada, M.; Ehara, M.; Toyota, K.; Fukuda, R.; Hasegawa, J.; Ishida, M.; Nakajima, T.; Honda, Y.; Kitao, O.; Nakai, H.; Klene, M.; Li, X.; Knox, J. E.; Hratchian, H. P.; Cross, J. B.; Adamo, C.; Jaramillo, J.; Gomperts, R.; Stratmann, R. E.; Yazyev, O.; Austin, A. J.; Cammi, R.; Pomelli, C.; Ochterski, J. W.; Ayala, P. Y.; Morokuma, K.; Voth, G. A.; Salvador, P.; Dannenberg, J. J.; Zakrzewski, V. G.; Dapprich, S.; Daniels, A. D.; Strain, M. C.; Farkas, O.; Malick, D. K.; Rabuck, A. D.; Raghavachari, K.; Foresman, J. B.; Ortiz, J. V.; Cui, Q.; Baboul, A. G.; Clifford, S.; Cioslowski, J.; Stefanov, B. B.; Liu, G.; Liashenko, A.; Piskorz, P.; Komaromi, I.; Martin, R. L.; Fox, D. J.; Keith, T.; Al–Laham, M. A.; Peng, C. Y.; Nanayakkara, A.; Challacmobe, M.; Gill, P. M. W.; Johnson, B.; Chen, W.; Wong, M. W.; Gonzalez, C.; Pople, J. A. *Gaussian 03*, revison D.01; Gaussian, Inc.: Wallingford, CT, 2003.

[7] Zeng, X. Q.; Beckers, H.; Neuhaus, P.; Grote, D.; Sander, W. *Z. Anorg. Allg. Chem.* **2012**, *638*, 526–533.

[8] Jacox, M. E. *J. Mol. Spectrosc.* **1980**, *80*, 257–271.

[9] Alvarez, R. M. S.; Cutín, E. H.; Mack, H. -G.; Védova, C. O. D. *J. Mol. Struct.* **1994**, *323*, 29–38.

[10] Qureshi, A. M.; Carter, H. A.; Aubke, F. *Can. J. Chem.* **1971**, *49*, 35–44.